JPE 17-2-5

https://doi.org/10.6113/JPE.2017.17.2.358
ISSN(Print): 1598-2092 / ISSN(Online): 2093-4718

A Novel Filtering Method Based on a Nonlinear Tracking Differentiator for the Speed Measurement of Direct-drive Permanent Magnet Traction Machines

Gaolin Wang†, Bowen Wang*, Nannan Zhao*, and Dianguo Xu**

†,*School of Electrical Engineering and Automation, Harbin Institute of Technology, Harbin, China

Abstract

This paper presents a novel filtering method for speed measurements to improve the low-speed performance of the direct-drive permanent magnet traction machines for elevators. Based on the theory of nonlinear tracking differentiator (NTD), this method, which can act as a high performance filter of a raw speed signal, obtains a more accurate speed feedback signal when applying a low-resolution encoder. In addition, it can relieve the interference caused by the position derivative for speed sampling. By analyzing the frequency response of the NTD, the influence of its parameters on the performance of the speed filtering is investigated. Compared with different types of low-pass filters, the proposed method shows a shorter time delay and a stronger ability in terms of noise suppression when the parameters are selected carefully. In addition, when using the measured speed signal through a nonlinear tracking differentiator as the feedback of the system, the motor runs more steadily at low speeds. As a result, the riding comfort of a direct-drive elevator can be improved. The feasibility of the proposed strategy was verified on an 11.7kW elevator traction machine using a commercial inverter.

Key words: Elevator, Low speed, Nonlinear tracking differentiator, Permanent magnet traction machine, Speed measurement

I. INTRODUCTION

Permanent magnet synchronous motors (PMSMs) have been applied widely due to their advantages in terms of high power density, high torque-to-inertia ratio, and high efficiency [1], [2]. Recently, they have been adopted more popularly in the gearless elevators of modern buildings [3]. Compared with traditional systems, PMSM based gearless elevators show high performance at start-up, stopping and moving, and can be designed more compactly [4]. Safety, stability and comfort are the essential demands of elevator systems [5]. To achieve a good riding comfort, accurate speed feedback should be obtained in real time for the closed-loop control system of a PMSM. However, during low speed operation, strong jerks can be caused by inaccuracies and large time delays of the speed feedback, which result in the discomfort of the passengers [6]. Poor speed performance can be improved by installing a high precision encoder, while the cost of system is inevitably increased.

Quadrature Encoder Pulse (QEP) sensors and linear hall sensors are widely used in PMSMs to obtain speed information. Several methods have been proposed to increase measurement accuracy when low-resolution QEP sensors are adopted. One promising scheme, presented in [7], is the so called the rotor position extrapolation algorithm using a polynomial estimator. This scheme was applied in the drive system proposed in [8], which analyzed the extrapolation scheme in terms of its speed and extrapolated rotor position performance through both simulation and experimental verifications. In [9], the instantaneous speed was estimated by a Luenberger observer based on a motion model of a PMSM. Then, the estimation error was corrected by the angular position obtained by the synchronous or asynchronous

Manuscript received Aug. 26, 2016; accepted Jan. 13, 2017
Recommended for publication by Associate Editor Bon-Gwan Gu.
†Corresponding Author: wgl818@hit.edu.cn
Tel: +86-451-86413420, Harbin Institute of Technology
*School of Electrical Engineering and Automation, Harbin Institute of Technology, China

sampling method. Compared to conventional observers, this method improves the resolution of the instantaneous velocity especially in the low speed region. The rotor position signal obtained by hall sensors often contains large harmonic components, which can influence the accuracy of the speed [10]. In order to remove high-order harmonics, a novel rotor position detection method based on the Synchronous Frequency Extractor (SFE) was utilized in [11], which was confirmed to effectively reduce the estimation error. In [12], an improved method using the periodic timer interrupt function and a simplified estimation to obtain position information based on hall sensors was presented.

In this paper, a novel filtering method adopting a Nonlinear Tracking Differentiator (NTD) is proposed for direct-drive permanent magnet traction machines, which tracks the speed signal more accurately. After analyzing the limitations of conventional speed measurement methods for low speed operations, the NTD based digital filter is adopted to achieve effective speed measurement at low speeds. Then the parameter selection of the proposed digital filter is discussed by analyzing the basic theory and frequency characteristic of the NTD. This shows a higher performance that relieves the time delay and suppresses external disturbances. Simulation and experimental results verify the feasibility of the proposed speed measurement method on an 11.7kW elevator machine.

II. Proposed Filtering Strategy Based on a Nonlinear Tracking Differentiator

A. Limitation of the Conventional Speed Calculation

The permanent magnet traction machine of an elevator should operate at ultra-low speeds to satisfy the demands of riding comfort, and the speed should decrease to 0.5rpm. To assure the good performance of the system, accurate speed information is expected in such situations.

Generally, the average speed is detected with the M, T or M/T method. The M method is often suitable for high speed calculations, while the T method is commonly used in low speed calculation. On the other hand, both high and low speeds can be calculated by the M/T method. However, a large detection delay is caused by the T method and M/T method when calculating ultra-low speeds, because the encoder pulse interval is much longer than the speed sampling period [13].

If the encoder generates 2048 signals per revolution, there are 8192 incremental count values per revolution after the quadrature processing. This means that the speed between two count pulses can be expressed as:

$$n = \frac{60}{8192 * T} \tag{1}$$

where n represents the average speed, and T represents the interval of the pulses. When n=7.32rpm, T is calculated to be 1ms, and when n=0.5rpm, T will be 14.65ms, while the sampling time of the speed loop is 1ms. Fig. 1 shows the relationship between the encoder pulse and the speed sampling period during ultra-low speed operation when the speed is 0.5rpm, where T_s is the sampling time of the speed loop. It can be seen that the speed is calculated after more than 14 execution cycles of the speed loop, which causes a large time delay. This delay deteriorates the dynamic response of the system, resulting in instability. Furthermore, large vibrations may occur during the steady state, which is not allowed in elevator applications. If a higher resolution encoder is used to avoid the time delay, it increases the cost. However, when the speed is calculated by the M method, the sampling time is fixed. The time delay is smaller when T_s is set shorter. Although the encoder pulses may not change in several sampling cycles during low speed, the average speed can be obtained by the low-pass filtering method.

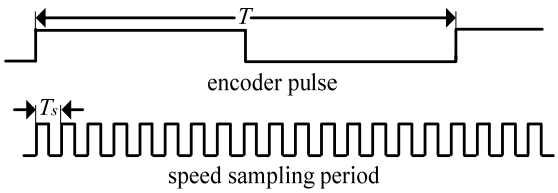

Fig. 1. Relation between the encoder pulse and the speed sampling period at low speed operation.

When getting the raw speed by the M method, a digital filter should be used before it feeds back to the speed controller. Low-pass filters (LPFs) are widely used in conventional speed estimation, whose filtering performance can be regulated by changing the cut-off frequency. The lower the cut-off frequency is, the smoother the filtered signal becomes. However, this can also result in a larger time delay. Therefore, an advanced filtering method based on the nonlinear tracking differentiator (NTD) is proposed in this paper to overcome the disadvantages of the LPF and to track the actual speed more effectively.

B. Speed Measurement Method Based on the NTD Theory

The NTD was originally proposed by Prof. Han [14]. It is mainly used to extract continuous signals and differential signals from non-continuous signals that have interference by noise. By using a nonlinear function, the method adopts integral calculation instead of differentiation, which suppresses the noise amplification. Furthermore, the input of the NTD is the discrete position signal, which is suitable for both incremental and absolute encoders. The principle of the NTD is described as follows.

For a double integral plant:

$$\begin{cases} \dot{x}_1 = \dot{x}_2 \\ \dot{x}_2 = u(x_1, x_2), \ u \le M \end{cases}, \tag{2}$$

a suitable $u(x_1, x_2)$ can be selected to guarantee a fast convergence from x_1 and x_2 to 0. Let $x_1 = x_1 - v$, this solution satisfies $\lim_{t\to\infty} x_1(t) = v, \lim_{t\to\infty} x_2(t) = \dot{v},$ where x_1 is the

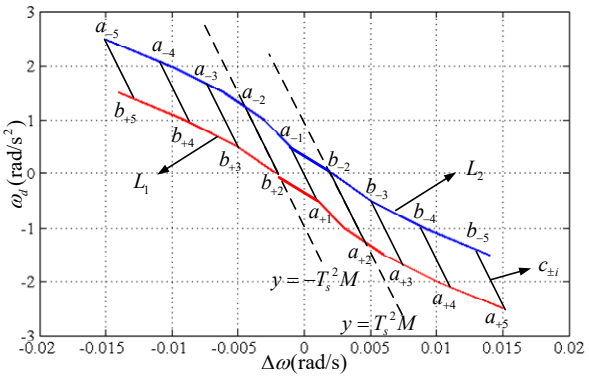

Fig. 2. Coordinate curves of initial value.

desired trajectory of v, and x_2 is its derivative. This means that when v is regarded as the input of the system, it is tracked quickly and effectively by x_1. Instead of containing all of the information of v, x_1 can extract its effective and continuous signal. Several adjustable parameters are included in $u(x_1, x_2)$. By changing these parameters, the filtering performance can be improved. $u(x_1, x_2)$ is the so-called optimal control synthesis (OCS) function which introduces considerable numerical errors into discrete-time implementations. (2) can be discretized as:

$$\begin{cases} x_1(k+1) = x_1(k) + T_s x_2(k) \\ x_2(k+1) = x_2(k) + T_s u(k) \end{cases}. \tag{3}$$

Based on the analysis above, the NTD for speed measurements is defined as:

$$\begin{cases} \omega_n(k+1) = \omega_n(k) + T_s \omega_d(k) \\ \omega_d(k+1) = \omega_d(k) + T_s fst(\omega_n(k) - \omega(k), \omega_d(k), M, h) \end{cases} \tag{4}$$

where M is the convergence factor, h is the filtering factor , ω is the raw speed, ω_n is the speed processed by the NTD, and ω_d is its derivative. $fst(\omega_n(k)\text{-}\omega(k), \omega_d(k), M, h)$ is a nonlinear OCS function of the NTD filtering part. The parameters M and h influence the dynamic performance and ability of the noise suppression, respectively.

$fst(\omega_n(k)\text{-}\omega(k), \omega_d(k), M, h)$ is a OCS function which is selected to obtain fast convergence of the NTD. Considering that the practical system is discretely calculated by the processing chip, it is more suitable to deduce the expression of $fst(\omega_n(k)\text{-}\omega(k), \omega_d(k), M, h)$ under the condition of discretization. Based on the theory of optimum time control, the expression of $fst(\omega_n(k)\text{-}\omega(k), \omega_d(k), M, h)$ can be deduced as follows.

Let $\Delta\omega(k)=\omega_n(k)\text{-}\omega(k)$ and assume that the initial value is $\boldsymbol{\omega} = [\Delta\omega(0), \omega_d(0)]^T$. Then after k steps of iterations, the solution of (4) is:

$$\begin{bmatrix} \Delta\omega(k) \\ \omega_d(k) \end{bmatrix} = \begin{bmatrix} 1 & kT_s \\ 0 & 1 \end{bmatrix} \begin{bmatrix} \Delta\omega(0) \\ \omega_d(0) \end{bmatrix} + \begin{bmatrix} 1 & (k-1)T_s \\ 0 & 1 \end{bmatrix} \begin{bmatrix} 0 \\ T_s \end{bmatrix} fst(0) + \ldots + \begin{bmatrix} 1 & T_s \\ 0 & 1 \end{bmatrix} \begin{bmatrix} 0 \\ T_s \end{bmatrix} fst(k-2) + \begin{bmatrix} 0 \\ T_s \end{bmatrix} fst(k-1) \tag{5}$$

Assuming:

$$\begin{bmatrix} \Delta\omega(k) \\ \omega_d(k) \end{bmatrix} = \begin{bmatrix} 0 \\ 0 \end{bmatrix}, \tag{6}$$

The expression of the initial values can be expressed as:

$$\begin{bmatrix} \Delta\omega(0) \\ \omega_d(0) \end{bmatrix} = \begin{bmatrix} kT_s^2 \\ -T_s \end{bmatrix} fst(k-1) + \begin{bmatrix} (k-1)T_s^2 \\ -T_s \end{bmatrix} fst(k-2) + \ldots + \begin{bmatrix} 2T_s^2 \\ -T_s \end{bmatrix} fst(1) + \begin{bmatrix} T_s^2 \\ -T_s \end{bmatrix} fst(0) \tag{7}$$

According to (7), when $fst(i)(i=0,1,\ldots k\text{-}1)=+M$, the collection of initial points $\{a_{+k}\}$ can be expressed as:

$$\begin{bmatrix} \Delta\omega \\ \omega_d \end{bmatrix} = \begin{bmatrix} \frac{1}{2}k(k+1)T_s^2 M \\ -kT_s M \end{bmatrix}. \tag{8}$$

When $fst(i)(i=0,1,\ldots k\text{-}1)= \text{-}M$, the collection of initial points $\{a_{-k}\}$ can be expressed as:

$$\begin{bmatrix} \Delta\omega \\ \omega_d \end{bmatrix} = \begin{bmatrix} -\frac{1}{2}k(k+1)T_s^2 M \\ kT_s M \end{bmatrix}. \tag{9}$$

When $fst(k\text{-}1)=+M$, $fst(i)=\text{-}M(i=0,1,\ldots k\text{-}2)$, the collection of initial points $\{b_{+k}\}$ can be expressed as:

$$\begin{bmatrix} \Delta\omega \\ \omega_d \end{bmatrix} = \begin{bmatrix} -\frac{1}{2}k(k+1)T_s^2 M - 2T_s^2 M \\ (k-2)T_s M \end{bmatrix}. \tag{10}$$

When $fst(k\text{-}1)=\text{-}M$, $fst(i)=+M(i=0,1,\ldots k\text{-}2)$, the collection of initial points $\{b_{-k}\}$ can be expressed as:

$$\begin{bmatrix} \Delta\omega \\ \omega_d \end{bmatrix} = \begin{bmatrix} \frac{1}{2}k(k+1)T_s^2 M - 2T_s^2 M \\ -(k-2)T_s M \end{bmatrix}. \tag{11}$$

Fig. 2 shows the location of a_{+k}, a_{-k}, b_{+k} and b_{-k}.

***Definition 1*: *SA*(k)**

SA(k) is the synchronous area of the amount of initial points $\boldsymbol{\omega}$. These points converge to the origin in k steps of iterations. ***SA***(k) is a convex polygon with $2k$ lines. For example, ***SA***(1) is the line of $a_{+1}a_{-1}$, while ***SA***(2) is the parallelogram of $a_{-2}b_{-2}a_{+2}b_{+2}$, and so on.

***Definition 2*: $\mathbf{L_1}$, $\mathbf{L_2}$**

Denote the fold lines a_{+k}, $a_{+(k-1)}$, ..., a_1, b_2, ..., $b_{+(k-1)}$,b_{+k} as $\mathbf{L_1}$ and a_{-k}, $a_{-(k-1)}$, ..., a_{-1}, b_{-2}, ..., $b_{-(k-1)}$,b_{-k} as $\mathbf{L_2}$. As analyzed above, when $\boldsymbol{\omega}$ is on or beneath $\mathbf{L_1}$, the control value fst is selected as $+M$; when $\boldsymbol{\omega}$ is on or above $\mathbf{L_2}$, fst is selected as $\text{-}M$; and when $\boldsymbol{\omega}$ is between $\mathbf{L_1}$ and $\mathbf{L_2}$, fst is selected in $[\text{-}M, +M]$.

As can be seen from Fig. 2, the state variable of the system converges to 0 in limited sampling periods through its relevant trajectory when $fst(i)$ changes under different rules. For example, if the initial point of $\boldsymbol{\omega}$ is above $\mathbf{L_2}$, fst will be selected as $\text{-}M$. Under the control force of fst, the point will move to $\mathbf{L_2}$. Then it will converge to 0 in limited sampling periods along its specific area. In particular, when the points are in the middle of lines a_ib_{-i} and $a_{-i}b_i$, fst is selected as 0,

which means that they will move to $a_{\pm i}$ without a control force.

The name the midpoint of a_ib_{-i} and $a_{-i}b_i$ is $c_{\pm i}$, which is shown in Fig.2. Thus, the coordinate of c_{+k} and c_{-k} can be expressed as:

$$\begin{bmatrix}\Delta\omega\\ \omega_d\end{bmatrix}=\begin{bmatrix}\frac{1}{2}k(k+1)T_s{}^2M-T_s{}^2M\\ -(k-1)T_sM\end{bmatrix} \tag{12}$$

and:

$$\begin{bmatrix}\Delta\omega\\ \omega_d\end{bmatrix}=\begin{bmatrix}-\frac{1}{2}k(k+1)T_s{}^2M+T_s{}^2M\\ (k-1)T_sM\end{bmatrix}. \tag{13}$$

Condition 1: Beyond ***SA***(2)

When the initial points are beyond ***SA***(2), the OCS function *fst*1 can be deduced as follows.

As can be concluded from (8)-(13), these points can be contained by the six parabolas that follow:

$$\begin{cases}\Delta\omega=\dfrac{\omega_d^2-T_sM\omega_d}{2M},\omega_d<0\\ \Delta\omega=-\dfrac{\omega_d^2-T_sM\omega_d}{2M},\omega_d>0\\ \Delta\omega=\dfrac{\omega_d^2-5T_sM\omega_d+2T_s{}^2M^2}{2M},\omega_d<0\\ \Delta\omega=-\dfrac{\omega_d^2-5T_sM\omega_d+2T_s{}^2M^2}{2M},\omega_d>0\\ \Delta\omega=\dfrac{\omega_d^2-3T_sM\omega_d}{2M},\omega_d<0\\ \Delta\omega=-\dfrac{\omega_d^2-3T_sM\omega_d}{2M},\omega_d>0\end{cases}. \tag{14}$$

Define $y=\Delta\omega+T_s\omega_d$, and (14) can be rewritten by three equations which can be expressed as:

$$\begin{cases}\omega_d-sign(y)\dfrac{M}{2}(T_s-\sqrt{\dfrac{8|y|}{M}+T_s{}^2})=-sign(y)T_sM & (a_{\pm i})\\ \omega_d-sign(y)\dfrac{M}{2}(T_s-\sqrt{\dfrac{8|y|}{M}+T_s{}^2})=sign(y)T_sM & (b_{\pm i})\\ \omega_d-sign(y)\dfrac{M}{2}(T_s-\sqrt{\dfrac{8|y|}{M}+T_s{}^2})=0 & (c_{\pm i})\end{cases} \tag{15}$$

Define the auxiliary equation as:

$$g(\omega_d,y)=\omega_d-sign(y)\frac{M}{2}(T_s-\sqrt{\frac{8|y|}{M}+T_s{}^2}). \tag{16}$$

It can be known that $g(c_{+i})=g(c_{-i})=0$, $g(a_{+i})=g(b_{+i})=T_sM$, and $g(a_{-i})=g(b_{-i})=-T_sM$.

According to the analysis above and by applying the power function in nonlinear control, the OCS function beyond ***SA***(2) can be obtained as:

$$fst1=\begin{cases}-Msign(g(\omega_d,y)), & |g(\omega_d,y)|\ge T_sM\\ -\dfrac{g(\omega_d,y)}{T_s}, & |g(\omega_d,y)|<T_sM\end{cases}. \tag{17}$$

This guarantees fast convergence from ω_n to ω, which means that the effective and continuous signal of the speed will be extracted accurately and fast.

Condition 2: Inside ***SA***(2)

It can be seen from Fig. 2 that ***SA***(2) is surrounded by 4 fold lines, whose expression are written as:

$$\begin{cases}y+T_s\omega_d=T_s^2M, & (a_{-2}b_{-2})\\ y+T_s\omega_d=-T_s^2M, & (a_{+2}b_{+2})\\ y=T_s^2M, & (a_{+2}b_{-2})\\ y=-T_s^2M, & (a_{-2}b_{+2})\end{cases}. \tag{18}$$

When k=2, the solution of *fst*(0) can be obtained from (7) as:

$$fst(0)=\frac{\Delta\omega(0)+2T_s\omega_n(0)}{T_s^2}=\frac{\omega_d(0)+y(0)/T_s}{T_s}. \tag{19}$$

Combining (18) and (19), the OCS function inside ***SA***(2) can be obtained as:

$$fst2=\frac{\omega_d+y/T_s}{T_s}. \tag{20}$$

where $|\omega_d+y/T_s|\le T_sM$, $|y|\le T_s^2M$.

Above all, the OCS function in this paper is set as a sectional type. When the initial point is beyond ***SA***(2), *fst* is selected as the maximum value ($\pm M$) to move it towards the inner ***SA***(2). Then, *fst* is selected as *fst*2 to make it converge to the origin as quickly as possible.

In order to suppress noise in the input signal and to avoid chattering in the switch function, let $h=nT_s$, where n is the amplification of T_s. This means that the sampling step in the OSC function is increased, which helps to filter high-frequency signals but inevitably causes a time delay. h is an important parameter of the NTD, which is analyzed in detail in Part C.

As a result, the expression of the OSC function is obtained as:

$$fst(\omega_n(k)-\omega(k),\omega_d(k),M,h)=-\begin{cases}Ma/d, & |a|\le d\\ Msign(a), & |a|>d\end{cases} \tag{21}$$

where:

$$a=\begin{cases}\omega_d+y/h, & |y|\le d_0\\ \omega_d+\dfrac{a_0-d}{2}sign(y), & |y|>d_0\end{cases}, \tag{22}$$

$$\begin{cases}d=Mh\\ d_0=dh\\ y=\omega_n-\omega+h\omega_d\\ a_0=\sqrt{d^2+8M|y|}\end{cases}. \tag{23}$$

Based on the conclusion above, the closed-loop control system of an elevator is established where the NTD acts as a digital filter of raw speed, as is shown in Fig. 3.

C. Frequency-Response Analysis and Parameter Selection

The NTD is a nonlinear system as a result of using a

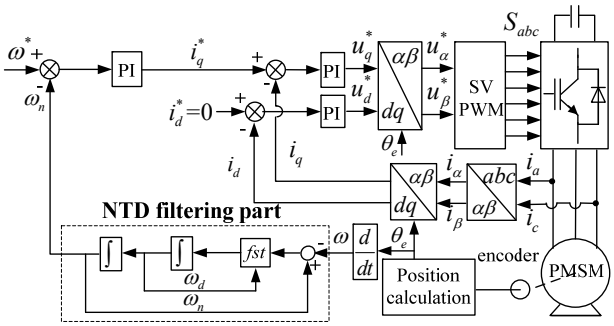

Fig. 3. Structure of the elevator traction machine drive.

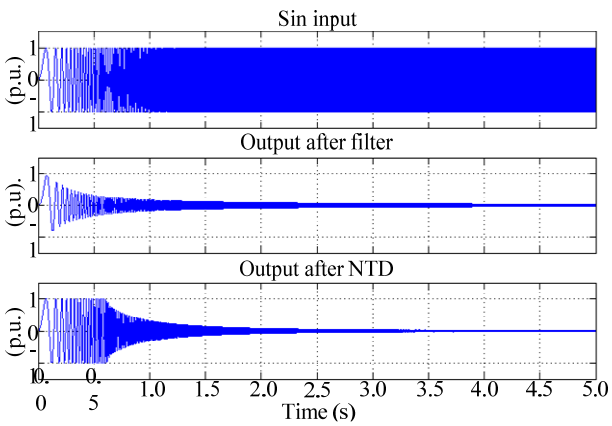

Fig. 4. Frequency sweep results of low-pass filter and NTD.

nonlinear function. Therefore, the conventional analysis methods of a linear system cannot be used to analyze its frequency characteristics. Here, a chirp signal is used to realize the frequency sweep measurement in order to obtain the frequency response of the NTD. Input the chirp signal to the NTD and observe its output. The frequency-response is obtained and compared with that of a first order Butterworth LPF, which shows the advantage of the NTD.

Note that the response of the NTD is related to the input amplitude, which should be considered in the sweep measurement. In the practical experimental platform, every variable whose range is from 0 to 1 is calculated by per unit values in the controller chip. When the input is between 0 and 1, the NTD shows the same characteristics because the amplitude of the input is in the same response interval. Therefore, the chirp signal is set to be 0~500Hz with its amplitude set 1. The NTD parameters are selected as follows: M=500 and h=0.01. The cut-off frequency of the first-order Butterworth LPF is 17Hz. The analysis results are shown in Fig. 4.

Note that the frequency of the chirp signal changes uniformly over time, meaning that the time in the horizontal axis can be regarded as the frequency, and the amplitude in vertical axis can be regarded as the gain of the system. Define the width in the horizontal axis when the amplitude drop is from 1 to 0.707 as the bandwidth. It can be seen that with an increase of the frequency, the amplitude of the LPF decreases

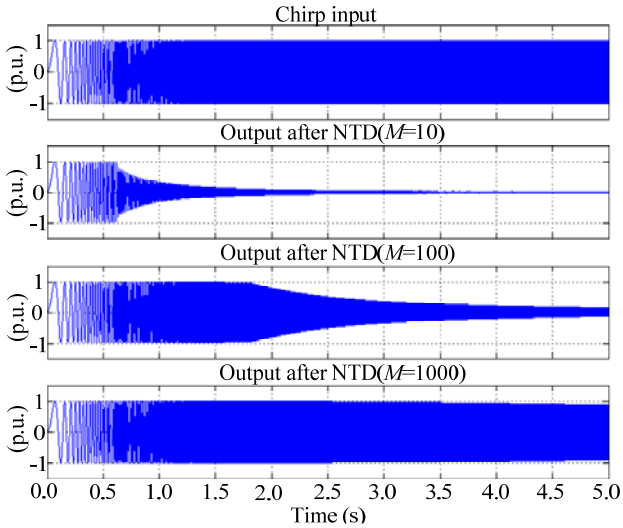

Fig. 5. Frequency sweep results of NTD using various M.

gradually which indicates a narrow bandwidth. Meanwhile the NTD shows a constant output amplitude during the low-frequency region and a wider bandwidth can be achieved. In addition, when reaching the cut-off frequency, the LPF shows slower attenuation ratio of amplitude when compared with that of the NTD. In conclusion, the NTD appears to have a better filtering property.

By using frequency sweep measurement, the influence of parameter M can be detected. Keeping h=0.01 and giving various values of M, different analysis results are shown in Fig. 5.

It can be illustrated that with an increase of M, the bandwidth becomes wider, which means that the NTD obtains a faster response and stronger stability. Generally, the bandwidth of the NTD will be proportional to $\sqrt{M}$.

As analyzed previously, M is the maximum value of the OCS function. When a larger value of M is selected, the force of the control variable to the system is stronger, which means a higher tracking speed. However, since M is proportional to the bandwidth of the system, a larger M does not assure the filtering effect of the high-frequency noise. According to [15], the scale of M can be selected from 500 to 1000 with no high-frequency existing.

Then by observing the output of the NTD when inputting a sinusoidal signal mixed with random noise, the filtering effects for different values of h can be detected. Set the frequency of standard sinusoidal signal as 1Hz and the amplitude as 1. The analysis results are shown in Fig. 6 when M=500, and h=5T_s, 10T_s, 20T_s and 30T_s respectively.

In Fig. 6, each of the four figures shows the expected output and the output of the NTD when the sinusoidal input contains random noise. It can be seen that the filtering performance of the NTD is improved significantly with the increasing of h, which means that it can perform better in extracting an effective signal.

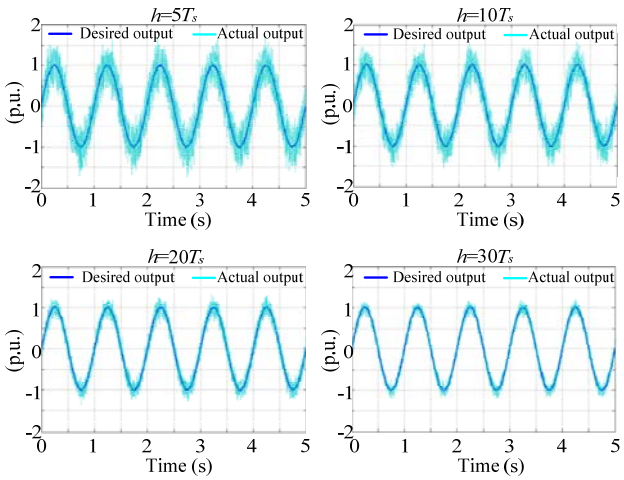

Fig. 6. Filtering effect of various *h*.

h mainly influences the effects of noise suppression. As analyzed before, $h=nT_s$, which enlarges the sampling step in the OSC function. Thus, the changing rate of the control variable is reduced. This means that when the input speed is in a higher frequency, the output remains unchanged instead of tracking it. Hence, the high frequency noise is filtered and the effective signal is extracted. However, the value of *h* should be limited because a time delay is present when it is selected to be larger. This affects the stability of the system when it is out of range. Therefore, *h* is usually selected from $3T_s$ to $20T_s$ in practical applications [14].

III. Simulation and Experimental Results

A. Simulation Results

A simulation has been carried out to compare the proposed filtering strategy in Matlab/Simulink. The parameters of the traction machine system used in simulation and experiment are the same, and are given in the Appendix.

The NTD parameters are selected as follows: M=1000, h=0.01, and the cut-off frequency of the Butterworth LPF is 17Hz because it is practically applied in the experimental platform. This set of the cut-off frequency assures both the rapidity and smoothness of the transient response. The PI control parameters are selected as follows: $K_{p\omega}$=3.61, $K_{i\omega}$=83.33, K_{pc}=37.49, and K_{ic}=575.04, which have been regulated to be optimal parameters. When the speed of the traction machine is changed from 0 to 2.5rpm, simulation results of the LPF and the NTD are shown in Fig. 7 and Fig. 8, respectively.

Fig. 7(a) and Fig. 8(a) show simulation results from 0 to 0.6s. It can be seen that the speed through the low-pass filter has a larger time delay (0.045s) than that of the NTD (0.022s), which influences stability when using it as the speed feedback. Fig. 7(b) and Fig. 8(b) show zoomed results of the speed. This detailed information can be compared to evaluate the performance in the steady state. From the results, the

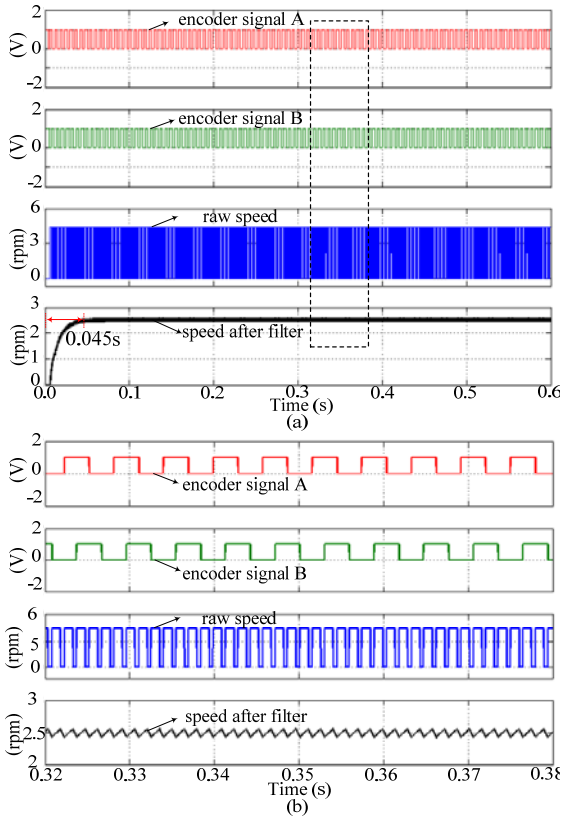

Fig. 7. Filtering results of the low-pass filter.

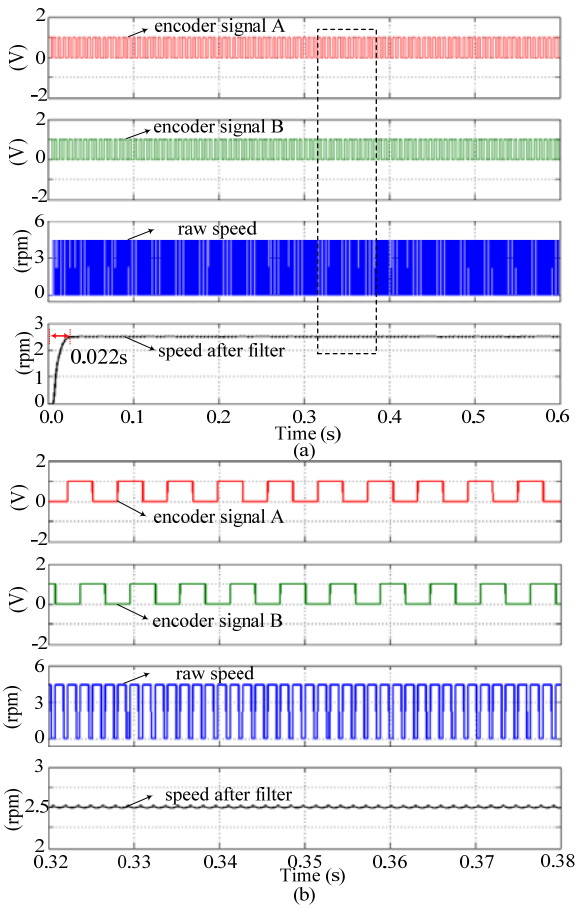

Fig. 8. Filtering results of the NTD.

(a) (b)

Fig. 9. Experimental platform of 11.7kW elevator traction machine. (a)Traction machines. (b) Drives.

speed signal obtained by using the NTD is smoother, with less vibration at low speeds.

B. Experimental Results

The proposed NTD filtering strategy was verified on an 11.7kW elevator traction machine using a commercial inverter. The experimental platform is shown in Fig. 9. A Sin-Cos encoder (ERN1387) with 2048 P/R is installed on the machine. The PWM frequency of the inverter is 6kHz. The whole control algorithm is executed by a STM32F103VB ARM chip. The control period of the speed loop is 1ms.

The performance of the tracking and filtering can be changed with different parameters of the NTD. In order to assure both the stability of the system and a rapid response, the NTD parameters are selected as follows: M=200, h=0.01, and the cut-off frequency of the LPF is still 17Hz. The regulated controlling parameters of the speed loop and current loop are $K_{p\omega}$=3.61, $K_{i\omega}$=83.33 and K_{pc}=37.49, K_{ic}=575.04, respectively. The machine shows acceptable vibration at the steady state, and achieves the response of speed loop and current loop as quickly as possible.

In order to evaluate the filtering effects of the proposed method, the accurate speed ω_{div} calculated from the position subdivision of the machine by a Sin-Cos encoder is introduced. According to this reference signal, the effects of the LPF and NTD will be compared intuitively.

1) Filtering effects of a first-order Butterworth LPF and the NTD: Accurate speed ω_{div} is used as the speed feedback. When the speed of the traction machine is 2.5rpm, the experimental waveforms are shown in Fig. 10 and Fig. 11.

Similar to the simulation results, the speed signal obtained by the NTD is smoother and shows a smaller time delay than that of the first-order Butterworth LPF, with less vibration at low speeds.

2) Control effect using the filtering speed as feedback: The speed subdivision ω_{div} can be regarded as the accurate speed of machine. Hence, it reflects the actual running situation. Using the filtered speed signal as the speed feedback of the machine, the practical control effects of the filtering methods can be obtianed from the experimental waveforms of ω_{div}. In order to verify the advantage of the proposed filtering strategy, different types of first-order LPFs (Butterworth,

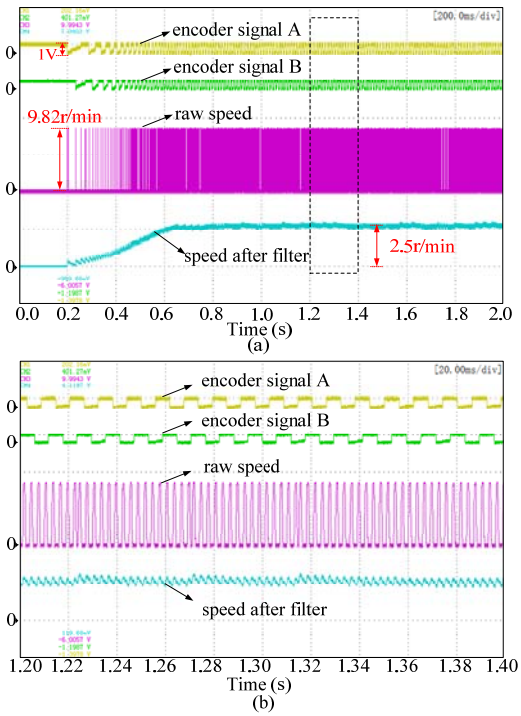

Fig. 10. Experimental results of LPF.

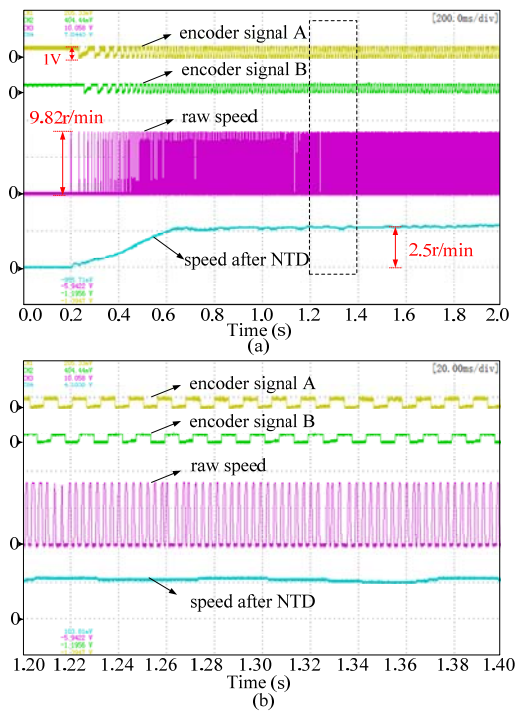

Fig. 11. Experimental results of NTD.

Chebyshev and Elliptic filters) were applied to calculate the speed in practical operation. The cut-off frequencies for all of the filters were set 17Hz. When the speed of the traction machine is 5rpm, the experimental waveforms are shown in Fig. 12. The second waveforms are the speed subdivision ω_{div}, and the bottom waveforms are the speed feedback.

It can be seen from Fig. 12(a)-(c) that the speed

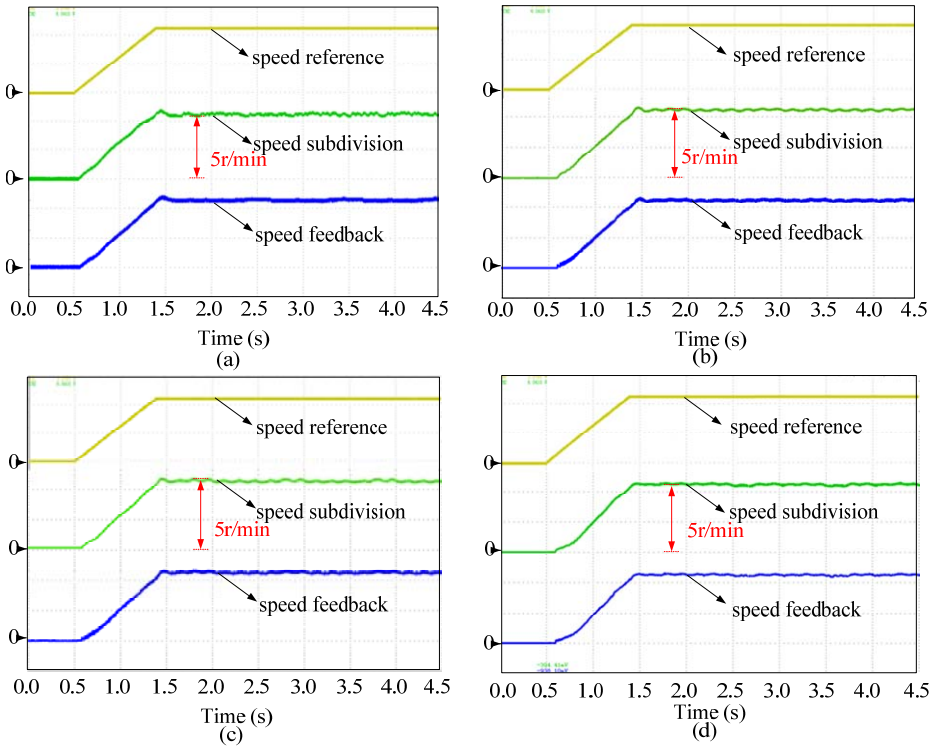

Fig. 12. Experimental results at 5rpm. (a) Butterworth LPF. (b) Chebyshev LPF. (c) Elliptic LPF.(d) NTD.

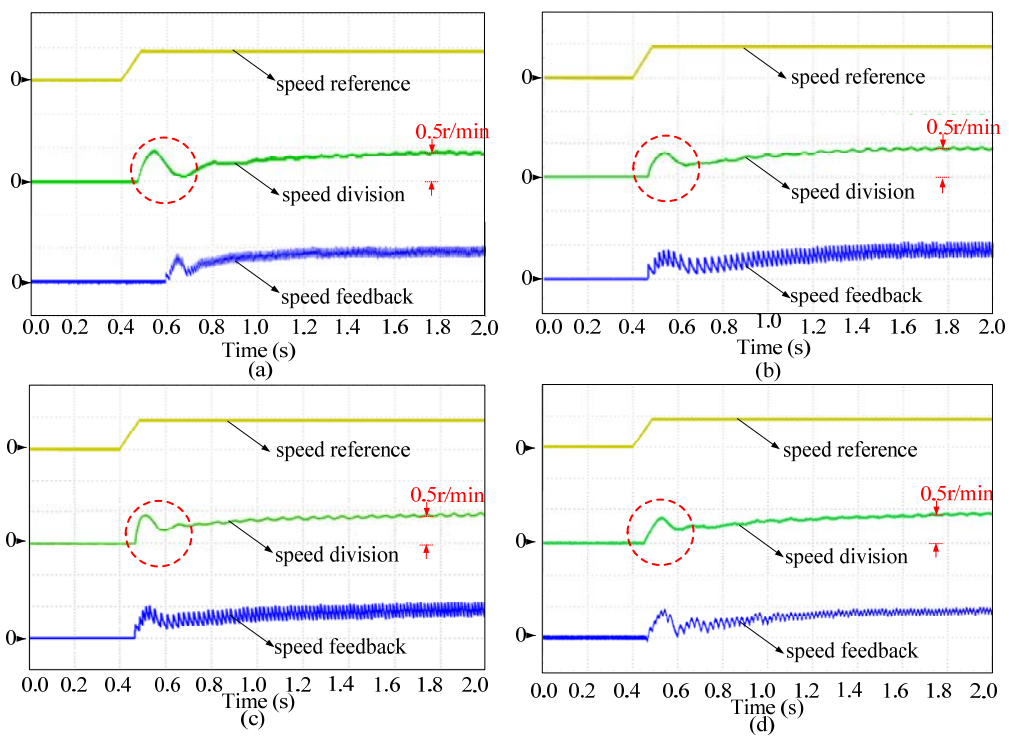

Fig. 13. Experimental results at 0.5rpm. (a) Butterworth LPF. (b) Chebyshev LPF. (c) Elliptic LPF. (d) NTD.

subdivisions ω_{div} when using LPFs of all types show overshoot during the rising process. This means a slight vibration of the traction machine. Furthermore, during the steady state, the speed is not stable enough due to the presence of obvious ripples. These will have impacts on the riding comfort of passengers. By contrast, the speed subdivision using the NTD is shown in Fig. 12(d). The results show a stable performance during the transient state without

any overshoot, and the speed is smoother in the steady state, ensuring the comfort of the passengers.

At ultra-low speed operation, when the speed reference is set as 0.5rpm, the experimental results are shown in Fig. 13. It can be seen from Fig. 13(a) and (c) that the speed subdivisions when using a Butterworth LPF and a Elliptic LPF contain serious vibrations in the transient state, which is highlighted in the figures. By contrast, the speed subdivisions using a Chebyshev LPF and the NTD display a relatively stable performance in the transient state. In terms of the transient state, there is no big difference between the Chebyshev LPF and the NTD. During the period of the steady state, there still exists a rotor vibration when using the Chebyshev LPF as shown in Fig. 13(b). However, it is reduced when using the NTD as shown in Fig. 13(d).

The stability of ultra-low speed is very important because it influences the comfort of passengers during start-up. In general, the NTD is a high efficiency filtering method with a smaller time delay and better filtering effects than other types of LPFs when its parameters are selected appropriately.

IV. Conclusion

A novel speed filtering method for permanent magnet traction machines to improve low speed performance is presented in this paper. Based on the theory of the nonlinear tracking differentiator (NTD), the method can relieve vibrations of the speed and reduce the time delay. Based on the analysis of the nonlinear OCS function and the impacts of its parameters, optimal parameters can be obtained which show more efficient performance and satisfy demands for stability. Furthermore, when using the speed signal through the nonlinear tracking differentiator as the feedback of a speed closed-loop control system, the motor shows a better performance compared with other types of low-pass filters. Therefore, smooth operation can be achieved at low speeds. Experimental results confirm the feasibility of the proposed strategy.

Appendix

TABLE I
Traction Machine Parameters

Parameters	value
Rated power	11.7kW
Rated voltage	380V
Rated current	23A
Rated speed	167rpm
Rated torque	670N·m
Stator resistance	0.23Ω
D-axis/Q-axis inductance	15mH
Number of pole pairs	12

Acknowledgment

Supported by the Research Fund for National Science Foundation of China (51522701), this research grants from Power Electronics Science and Education Development Program of Delta Environmental & Educational Foundation (DREK2015002), National Science and Technology Support Program (2014BAF08B05).

References

[1] A. B. Wang, Q. J. Wang, and W. D. Jiang. "A novel double-loop vector control strategy for PMSMs based on kinetic energy feedback," *Journal of Power Electronics*, Vol. 15, No. 5 pp. 1256-1263, Sep. 2015.

[2] J. W. Jung, Q. D. Dong, and T. T. Vu. "A nonlinear sliding mode controller for IPMSM drives with an adaptive gain tuning rule," *Journal of Power Electronics*, Vol. 15, No. 3 pp. 753-762, May. 2015.

[3] F. Liu, A.W. Shen, Y. N. Zhang, and W. B. Fu, "A rapid and high-accuracy control scheme of starting torque for elevators without a weight transducer," in *IEEE 23rd International Symposium on Industrial Electronics*, pp. 733-738, 2014.

[4] H. Yetis, H. Boztepeli, Y. Yasa, and E. Mese, "Comparative design of direct drive PM synchronous motors in gearless elevator systems," in *3rd International Conference on Electric Power and Energy Conversion Systems*, pp. 1-5, 2013.

[5] G. L. Wang, G. Q. Zhang, R. F. Yang, and D. G. Xu. "Robust low-cost control scheme of direct-drive gearless traction machine for elevators without weight transducer," *IEEE Trans. Ind. Appl.*, Vol. 48, No. 3, pp. 996-1005, May. 2012.

[6] B. Blanusa and B. Knezevic, "Optimal flux control of elevator drive," in *IEEE on Information, Communication and Automation Technologies*, pp. 1-6, 2013.

[7] Z. Feng and P. P. Acarnley, "Extrapolation technique for improving the effective resolution of position encoders in permanent-magnet motor drives," *IEEE Trans. Mechatron.*, Vol. 13, No. 4, pp. 410-415, Aug. 2008.

[8] S. Munggonrit, M. Konghirun, and K. Tungpimolrut, "Speed closed-loop drive system of permanent magnet synchronous motor using low-count QEP," in *International Conference on Electrical Engineering / Electronics Computer Telecommunications and Information Technology*, pp. 269-273, 2010.

[9] H. Li, H. Xie, X. Yi, and Y. Zheng, "Research on low speed control of permanent magnet synchronous motor based on state observer," in *4th International Conference on Biomedical Engineering and Information*, pp. 2018-2022, 2011

[10] X. Zhang and W. Zhang, "An improved rotor position estimation in PMSM with low-resolution hall-effect sensors," in *17th International Conference on Electrical Machines and Systems*, pp. 2722-2727, 2014.

[11] X. Song, J. Fang, and B. Han, "High-precision rotor position detection for high-speed surface PMSM drive based on linear hall-effect sensors," *IEEE Trans. Power Electron.*, Vol. 31, No. 7, pp. 4720-4731, Jul. 2016.

[12] Y. P. Yang and Y. Y. Ting, "Improved angular displacement estimation based on hall-effect sensors for

driving a brushless permanent-magnet motor," *IEEE Trans. Ind. Electron.*, Vol. 61, No. 1, pp. 504-511, Jan. 2014.
[13] F. Wu, S. M. Wan, S. H. Huang, and Y. J. Chen, "Study on speed detection and control method of PMSM under ultra-low speed," in *Universities Power Engineering Conference*, pp. 178-183, 2007.
[14] J. Han, "From PID to Active Disturbance Rejection Control," *IEEE Trans. Ind. Electron.*, Vol. 56, No. 3, pp. 900-906, Mar. 2009.
[15] G. L. Wang, Y. Wang, J. Xu, N.N. Zhao, and D. G. Xu, "Weight-transducerless rollback mitigation adopting enhanced MPC with extended state observer for direct-drive elevators," *IEEE Trans. Power Electron.*, Vol. 31, No. 6, pp. 4440-4451, Jun. 2016.

Gaolin Wang (M'13) received his B.S., M.S. and Ph.D. degrees in Electrical Engineering from the Harbin Institute of Technology (HIT), Harbin, China, in 2002, 2004 and 2008, respectively. In 2009, he joined the Department of Electrical Engineering, HIT as a Lecturer, where he has been a Full Professor of Electrical Engineering, since 2014. From 2009 to 2012, he was a Postdoctoral Fellow in the Shanghai Step Electric Corporation, Shanghai, China, where he was involved in traction machine control for direct-drive elevators. He has authored more than 60 technical papers published in journals and conference proceedings. He is the holder of 10 Chinese patents. His current research interests include permanent magnet synchronous motor drives, high performance direct-drives for traction systems, position sensorless control of AC motors, and efficiency optimization control of PMSMs. Dr. Wang serves as an Associate Editor of the *IET Electric Power Applications*, and the *Journal of Power Electronics*. He received an Outstanding Research Award and a Delta Young Scholar Award from the Delta Environmental and Educational Foundation, in 2012 and 2014, respectively.

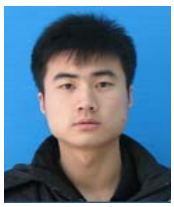

Bowen Wang received his B.S. degree in Electrical Engineering from the Harbin Institute of Technology (HIT), Harbin, China, in 2015. He is presently working towards his M.S. degree in Power Electronics and Electrical Drives in the School of Electrical Engineering and Automation, HIT. His current research interests include direct-drive permanent magnet synchronous motor control and position sensorless control.

Nannan Zhao received his B.S. and M.S. degrees in Control Science and Engineering from the Harbin Institute of Technology (HIT), Harbin, China, in 2013 and 2015, respectively. He is presently working towards his Ph.D. degree in Power Electronics and Electrical Drives in the School of Electrical Engineering and Automation, HIT. His current research interests include permanent magnet synchronous motor drives and the position sensorless control of AC motors.

Dianguo Xu (M'97, SM'12, Fellow' 17) received his B.S. degree in Control Engineering from the Harbin Engineering University, Harbin, China, in 1982; and his M.S. and Ph.D. degrees in Electrical Engineering from the Harbin Institute of Technology (HIT), Harbin, China, in 1984 and 1989, respectively. In 1984, he joined the Department of Electrical Engineering, HIT, as an Assistant Professor. Since 1994, he has been a Professor in the Department of Electrical Engineering, HIT. He was the Dean of the School of Electrical Engineering and Automation, HIT, from 2000 to 2010; and the Assistant President of HIT, from 2010 to 2014. He is presently working as the Vice President of HIT. His current research interests include renewable energy generation technology, power quality mitigation, sensorless vector controlled motor drives, and high performance PMSM servo systems. He has published over 600 technical papers in journals and conference proceedings. Dr. Xu is a Fellow of IEEE, an Associate Editor of the *IEEE Transactions on Industrial Electronics* and *IEEE Journal of Emerging and Selected Topics in Power Electronics*. He serves as the Chairman of IEEE Harbin Section.